

## Characterization of Submicron Exhaust Particles from Engines Operating Without Load on Diesel and JP-8 Fuels

C. Fred Rogers,<sup>1</sup> John C. Sagebiel,<sup>1</sup> Barbara Zielinska,<sup>1</sup> W. Patrick Arnott,<sup>1</sup>  
Eric M. Fujita,<sup>1</sup> Jacob D. McDonald,<sup>2</sup> James Brian Griffin,<sup>3</sup> Kerry Kelly,<sup>4</sup>  
Dana Overacker,<sup>4</sup> David Wagner,<sup>4</sup> JoAnn S. Lighty,<sup>4</sup> Adel Sarofim,<sup>4</sup>  
and Glenn Palmer<sup>5</sup>

<sup>1</sup>Desert Research Institute, Division of Atmospheric Sciences, University and Community College System of Nevada, Reno, Nevada

<sup>2</sup>Now at Lovelace Respiratory Research Institute, Albuquerque, New Mexico

<sup>3</sup>Now at Lam Research, Fremont, California

<sup>4</sup>Department of Chemical and Fuels Engineering, University of Utah, Salt Lake City, Utah

<sup>5</sup>Hill Air Force Base, Ogden, Utah

---

Diluted exhaust from a selection of Air Force ground support vehicles was subjected to gravimetric, carbon, and size distribution analyses in September 1999. The vehicles operated on diesel and JP-8 fuels. In most cases, the engines involved were similar to civilian counterparts. The tests involved “low” and “high” idle settings but no external loads were imposed. Particle size distribution data, obtained over the 10 to 352 nanometer diameter range using an SMPS instrument, showed that the relative number count of accumulation mode particles increased with respect to nucleation mode particles as the engine rpm increased. The SMPS distributions often explained the main variations in the integrated PM<sub>2.5</sub> gravimetric mass data. Particulate mass derived from the SMPS data and from cascade impactor measurements were well correlated (regression slope 1.02). Empirically determined “elemental” carbon (EC) and “organic” carbon (OC) were the main constituents of the PM<sub>2.5</sub> gravimetric mass (regression slope 0.89). EC contributed less, and OC contributed more to the PM<sub>2.5</sub> mass than was found in some recent studies of exhaust from vehicles operated under external loads. The observed particle nucleation modes were attenuated by coagulation with accumulation mode particles, but it does

not appear that artifact particle formation was operative in these experiments. The estimated  $\pm 1\sigma$  measurement precisions range from about  $\pm 4\%$  for the largest impactor mass concentration determinations to  $\pm 24\%$  for some of the SMPS mass concentration estimates.

---

### INTRODUCTION

This paper describes emissions measurements obtained on a variety of military vehicles at Hill Air Force Base (HAFB, near Ogden, UT) in September 1999. The purposes of the measurements were (1) to provide exhaust particle characterization data for a selection of Aircraft Ground Support Equipment (AGE) utilized at HAFB, and (2) to provide an independent data set relevant to developing advanced methods for monitoring emissions at Department of Defense facilities. Engines utilizing diesel and JP-8 aviation fuel were operated at constant rpm settings with no external loads imposed, i.e., the tests involved “low” and “high” idle conditions. The diesel engines were similar to civilian counterparts. This paper focuses on the results obtained from a subset of the total list of tests conducted for this project. Other runs not discussed here involved variable rpm settings and gasoline engine data that are mainly relevant to other project objectives.

Motor vehicle exhaust particles fall almost entirely in the PM<sub>2.5</sub> category and are mostly composed of graphitic or “elemental” carbon, together with less refractory or “organic” carbon (e.g., Kittelson 1998; Kleeman et al. 2000). The particles may also contain trace metals, inorganic ions, and other material. Exhaust particle size distributions are relevant to health concerns; it is hypothesized that ultrafine (i.e., less than 100 nm

---

Received 23 May 2001; accepted 12 September 2002.

This research was supported by Strategic Environmental Research and Development Program (SERDP) Project CP-1106, Characterization of Particulate Emission: Size Characterization and Chemical Speciation. The Desert Research Institute, University and Community College System of Nevada, worked under subcontract to the University of Utah in this project. We thank Mr. Bob Armstrong of Hill Air Force Base for his helpful cooperation. We also thank two anonymous reviewers for their careful and detailed comments.

Address correspondence to C. Fred Rogers, Desert Research Institute, Division of Atmospheric Sciences, University and Community College System of Nevada, 2215 Raggio Parkway, Reno, NV 89512. E-mail: fredr@dri.edu

**Table 1**  
Aircraft ground support equipment vehicles tested in the Hill AFB experiment

Vehicle type	Fuel type	Manufacture date	Engine specifications
Dodge Bobtail	Diesel	1996	Cummins, 5.9 liter, turbo
Coleman	Diesel	1997	Cummins, 5.9 liter, turbo
Bobtail	Diesel	1990	Cummins, 5.9 liter, turbo
Jammer JP-4 Model Z-790	JP-8	1992	HATZ, 1.27 liter (2 cylinder)

“Bobtail” and “Coleman” vehicles are designed for aircraft towing applications; “Jammers” are used to lift munitions into aircraft.

in diameter) particles deposit more efficiently in the lungs and are potentially more damaging than if the same chemical compounds were inhaled as larger particles (see review in Lighty et al. 2000). Kittelson (1998), Abu-Allaban et al. (2002), and other researchers have presented evidence for the existence of high concentrations of ultrafine particles in on-road studies of heavy-duty diesel engine exhaust. JP-8 aviation fueled engines have not been included in previous studies, to the best of our knowledge. The U.S. Department of Defense is looking into the merits of converting some types of diesel engines to run on this fuel.

This paper will present particulate size distributions and mass and carbon concentration data. The data were obtained with the engines at steady rpm, but with no load imposed, so the findings are relevant to idling situations, either on the flight line at HAFB or in an urban setting, rather than to driving under load. The engine parameters that could be controlled as independent variables were manufacture date, rpm, and fuel. The vehicles and engines selected for this study are not intended to represent a fleet average, although authorities at HAFB stated that they were reasonably representative of vehicles in use there. The intent of this paper is to show the variations in PM<sub>2.5</sub> mass and carbon concentrations together with the particle size distribution data that explain some of the observed variations. The HAFB study also included measurements of PAH compounds and real-time

determinations of particulate light absorption; those data will be presented in companion papers.

### EXPERIMENTAL APPROACH

The project (Strategic Environmental Research and Development Program, SERDP, sponsored by DOD, EPA, and DOE) objectives called for testing a representative set of AGE vehicles at HAFB, involving different engine types and fuels. The final AGE vehicle selection is shown in Table 1, in the order in which the measurements were conducted.

The engines had been maintained by procedures that met or exceeded their manufacturer’s specifications. Refinery data indicate that the diesel fuel used at HAFB at the time of this experiment contained 380 ppm sulfur by weight. A sample of the JP-8 fuel yielded a sulfur content of 96 ppm. The measurements were conducted at fixed engine throttle settings, and hence fixed rpm levels, as shown in Table 2. In all tests, the engines had been brought to stable operating temperature before the tests began. Based on the estimated time required to collect sample deposits sufficient for chemical analyses, the measurement run length was designated as 45 min.

The measurements at HAFB all utilized a diluted exhaust aerosol supply. Dilution is necessary in order to cool the hot exhaust with filtered air, and also to avoid water vapor condensation.

**Table 2**  
Vehicle and dilution test conditions for Hill AFB tests

Date	Run number*	Run time	AGE vehicle	Fuel	RPM	Dilution ratio
9/21/99	5	1604–1649	'96 Dodge bobtail	Diesel	800	1:18
9/22/99	6	937–1022	'97 Coleman	Diesel	800	1:19
9/22/99	7	1056–1141	'97 Coleman	Diesel	1800	1:19
9/22/99	8	1212–1257	'97 Coleman	Diesel	800	1:20
9/22/99	9	1704–1749	'90 Bobtail	Diesel	750	1:19
9/22/99	10	1816–1901	'90 Bobtail	Diesel	1200	1:19
9/23/99	11	950–1035	'90 Bobtail	Diesel	750	1:18
9/23/99	12	1127–1212	'90 Bobtail	Diesel	1700	1:19
9/23/99	13	1408–1453	Jammer	JP-8	2500	1:18

\*Runs 8 and 11 repeated earlier runs in order to provide replicates for chemical analyses.

The dilution source sampler was built at Desert Research Institute (DRI), based on the design of Hildemann et al. (1989); it is also somewhat similar to that used recently by Kleeman et al. (2000). The sample-to-filtered air dilution ratios are given in the last column of Table 2. Data presented in this paper are corrected back to estimated tailpipe values prior to dilution. Further details of the dilution sampler are given in Appendix A.

The exit ports on the dilution sampler aging chamber supplied four sampling trains, two of which are relevant to this paper. The first sampling train was connected to one of the cyclone ports, and led to two MOUDI cascade impactors (MOUDI, MSP Corp. St. Paul, MN). MOUDI #1 was used to expose Teflon substrates for subsequent gravimetric analyses, and MOUDI #2 was used to expose aluminum foil substrates for empirical particulate carbon analysis by the thermal-optical method (Chow et al. 1993). Each MOUDI utilized stages with the following cutoff diameters: 3.16, 1.78, 1.0, 0.54, 0.37, 0.148, 0.105, and 0.054 micrometers. The second dilution sampler port supplied a Scanning Mobility Particle Sizer (SMPS—Wang and Flagan 1990) and did not utilize a cyclone.

The SMPS was configured to perform repeated 90 s size distribution scans (60 s up scan, 30 s down scan) during each experiment run in case the distributions changed during the run. The SMPS sample flow was 0.7 l/m, and the sheath flow in its electrostatic classifier was 7.0 l/m. The SMPS used for these measurements was not configured with the standard length tub-

ing connection between the electrostatic classifier and its condensation nuclei counter; the aerosol transit time used in the data analysis (“delay time”) has been adjusted accordingly. The individual SMPS scans have been averaged over each experimental run. In most cases little variation was observed during the course of any one 45 min run. The data averages were generated by taking the arithmetic average of the six to seven determinations for each size distribution channel and averaging over the six to seven SMPS scans obtained during each run. (Appendix B lists the number of SMPS scans obtained and presents measures of the stability of SMPS data during each run).

**RESULTS**

***Size Distribution Measurements***

The following terminology is relevant to the SMPS data: the “nucleation mode,” 7.5 to 42 nm, and the “accumulation mode,” 42 to 1000 nm (Baumgard and Johnson 1996). Note that the SMPS instrument does not detect particles smaller than about 10 nm mobility-equivalent diameter. The quantity shown in the data reported here is the differential particle concentration per logarithmic size interval, or number of particles per cubic centimeter per log diameter interval.

The averaged data from Run 5 are shown in Figure 1. The nucleation mode peak diameter is 21 nm. An apparent

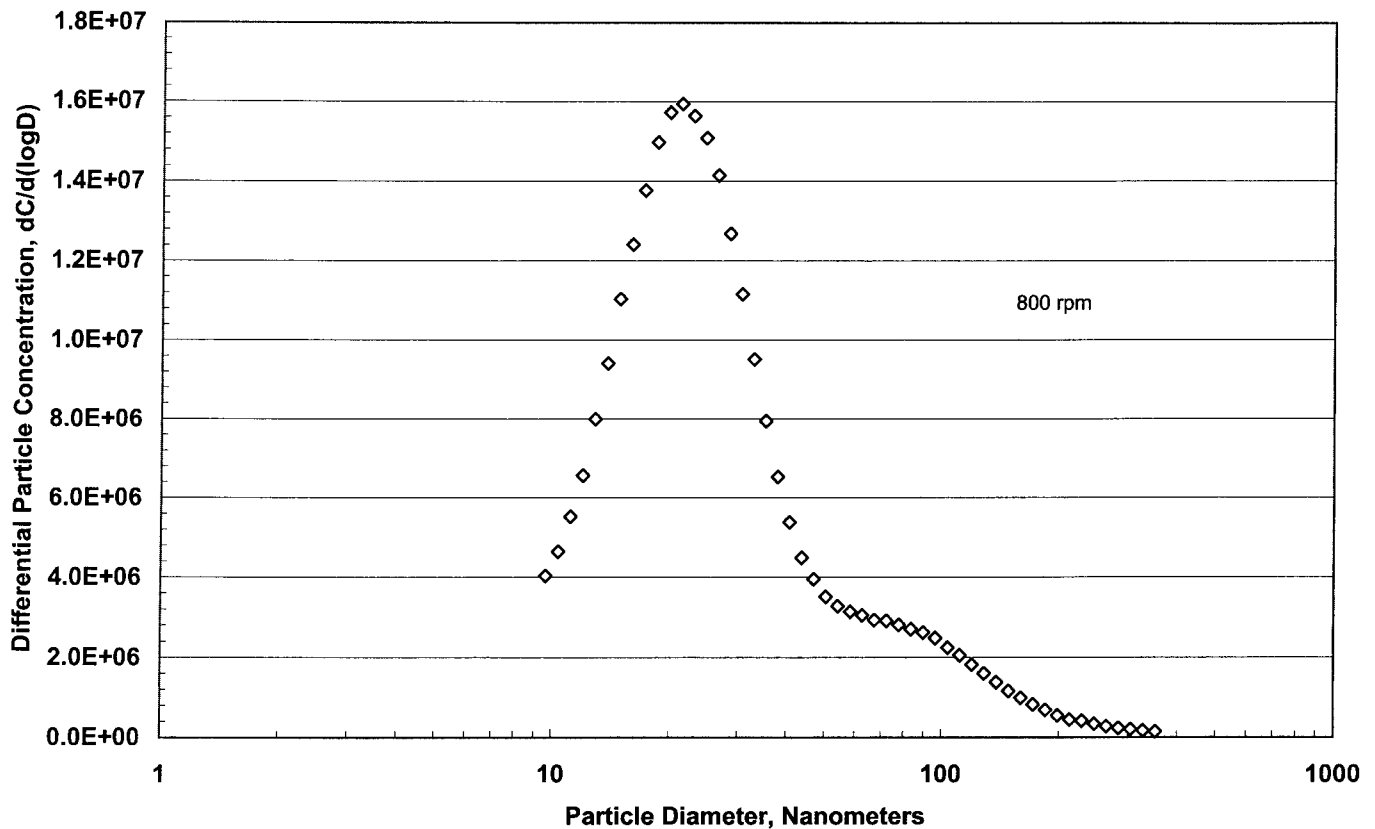


Figure 1. Run 5, 1996 Dodge Bobtail.

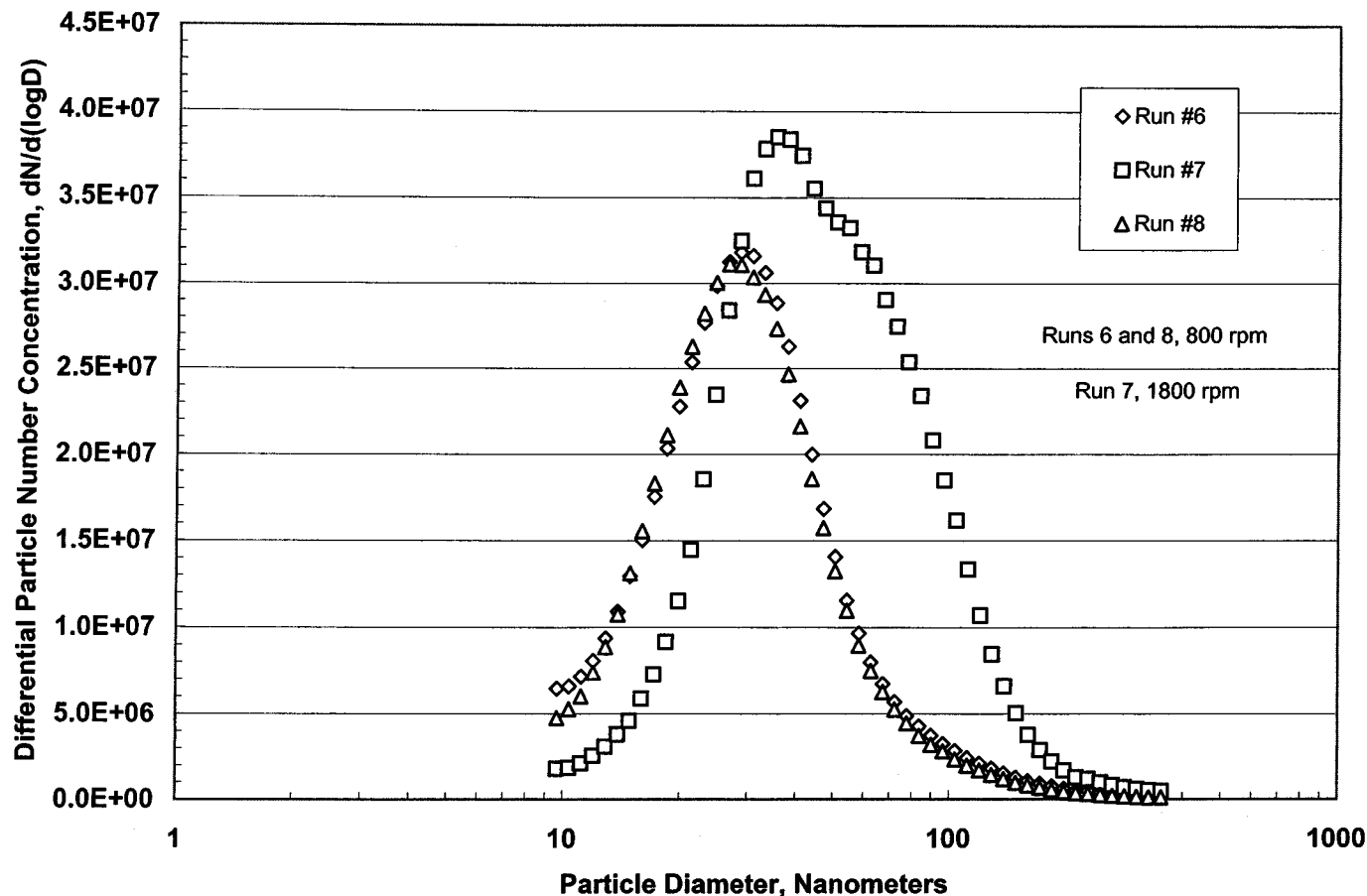


Figure 2. Runs 6, 7, and 8, 1997 Coleman.

accumulation mode can be resolved. The Count Median Diameter (CMD) is 22 nm, close to the peak diameter and confirming that most of the particle number counts are in the nucleation mode.

The averaged data from Runs 6, 7, and 8 (1997 Coleman) are shown in Figure 2. The distributions for Runs 6 and 8 show single modes peaking at 28 and 27 nm, respectively. The Count Median Diameters (CMD) for these two runs, calculated from the 51-channel differential distributions, equaled the peak diameters to within one nm, suggesting that the distributions are lognormal. Run 8 was a planned repeat of Run 6, with the engine at 800 rpm idle. Repeat runs allowed replicates of the most detailed organic chemical analyses, the results of which will be reported in companion papers. For Run 7, the engine rpm setting was raised to 1800 rpm. The size distribution for Run 7 exhibits an apparently bimodal structure, with the main peak at 37 nm and a second peak developing in the accumulation mode size region. The CMD for Run 7 was 43 nm.

The experiment plan called for testing the expected higher-emitting engines later in the test sequence, after the runs on the newer and cleaner engines. Runs 9–12 involved one of the older vehicles in the study, a 1990 diesel-fueled bobtail. The engine

was operated at 750 rpm for Run 9, 1220 rpm for Run 10, 750 rpm again for Run 11, and 1700 rpm for Run 12, generating the data shown in Figure 3. Run 11 was a repeat of Run 9. The peak diameters for Runs 9 and 11 were 25 and 28 nm, with CMD's of 26 and 30 nm, respectively. The nucleation mode peaked at 21 nm for Run 10, and an accumulation mode had developed; the CMD for Run 11 was 30 nm. The distribution for Run 12 peaked in the accumulation mode size range, at 67 nm. The calculated CMD for Run 12 was 63 nm.

Run 13 involved an air-cooled engine that can operate on either diesel or JP-8 aviation fuel. The averaged SMPS data are shown in Figure 4. This engine, at this rpm, generated some of the largest particles in the HAFB tests. The distribution exhibits a single mode peaking at 84 nm, with a CMD of 83 nm.

A summary of the averaged SMPS differential particle concentration distributions, including peak diameters, CMDs, and nucleation and accumulation mode particle number concentrations is presented in Table 3.

#### Particulate Mass Measurements

Size-resolved particulate mass data were obtained from microbalance determinations of the mass distributions on Teflon

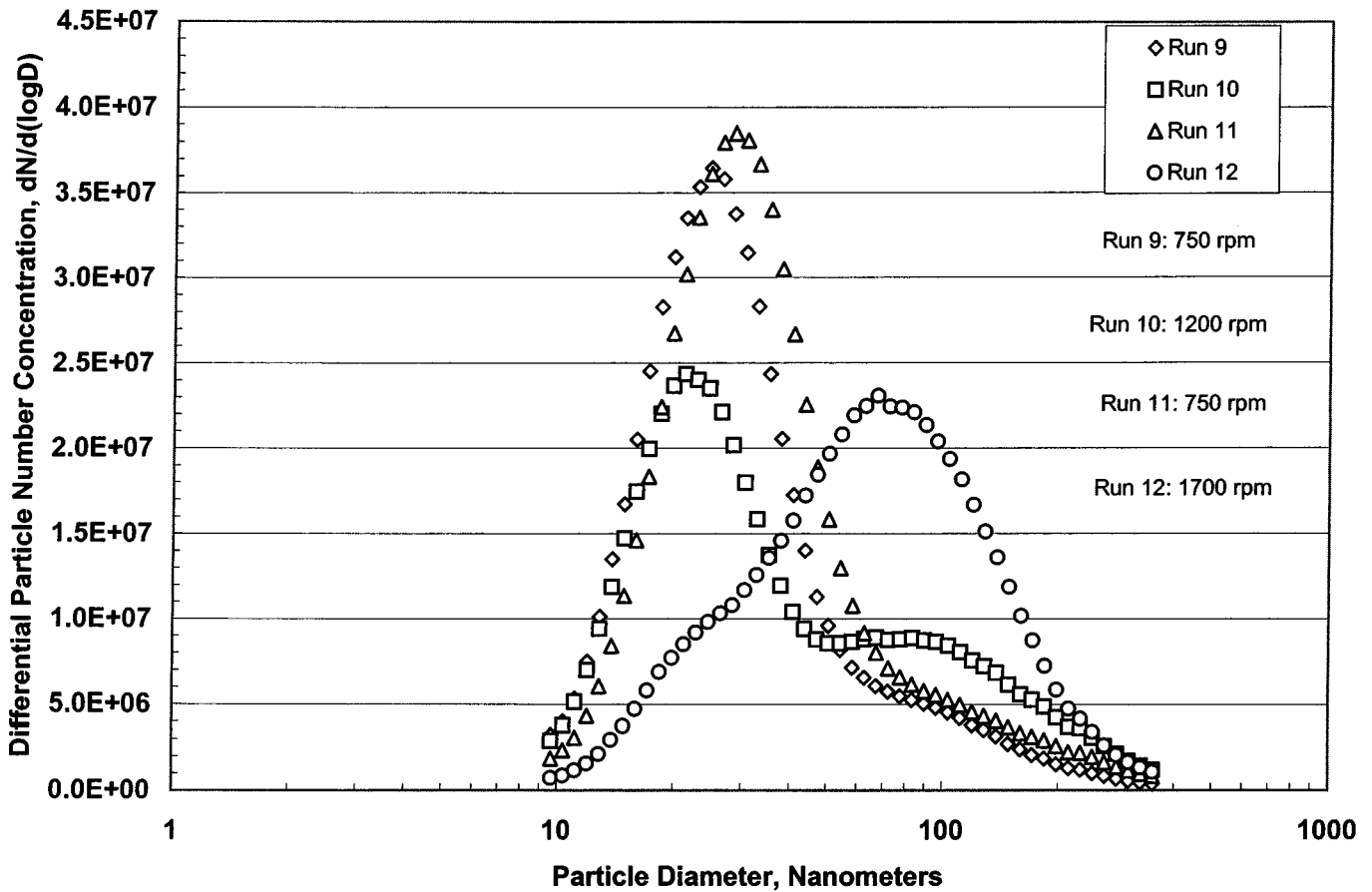


Figure 3. Runs 9, 10, 11, and 12, 1990 Bobtail.

substrates exposed in the eight stages of MOUDI impactor #1. Integrated mass concentrations were obtained by summing over all stages, but the 37 mm quartz afterfilter mass data are not included in the integrated mass sums because of potential gas-phase organic compound mass adsorption artifacts.

Integrated SMPS mass concentrations were estimated by converting the SMPS averaged differential number data to differential mass data, by assuming a particle specific gravity of unity and summing the resulting distributions. Shi et al. (2000) examined exhaust particle densities in detail, finding a range from

Table 3  
Summary of particle size distribution measurements during Hill AFB tests

Run number	Peak diameter, nm	CMD, nm	Nucleation mode particle concentration, cm <sup>-3</sup>	Accumulation mode particle concentration, cm <sup>-3</sup>	Total particle concentration, cm <sup>-3</sup>
5	21	22	6.88E+6	1.67E+6	8.54E+6
6	28	28	1.32E+7	3.94E+6	1.72E+7
7	37	43	1.12E+7	1.32E+7	2.44E+7
8	27	27	1.30E+7	3.56E+6	1.65E+7
9	25	26	1.44E+7	3.91E+6	1.83E+7
10	21	28	1.01E+7	5.92E+6	1.60E+7
11	28	30	1.44E+7	5.63E+6	2.01E+7
12	67	63	4.84E+6	1.25E+7	1.73E+7
13	84	83	3.01E+6	3.18E+7	3.49E+7

Nucleation mode data sum over 10 to 42 nm; accumulation mode data sum over 42 to 352 nm in SMPS distributions.

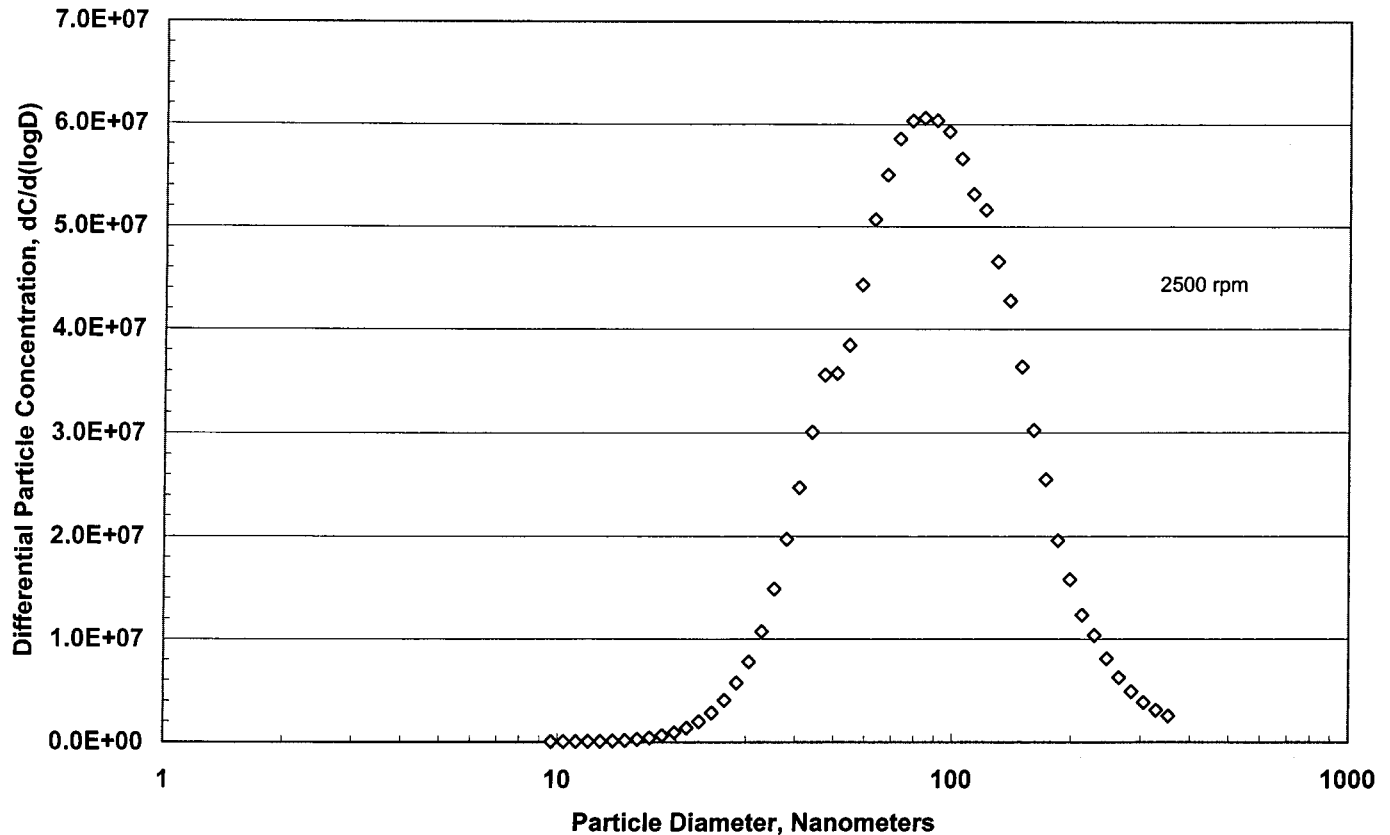


Figure 4. Run 13, JP-8 Jammer.

about less than 0.5 to greater than 2.0 g/cm<sup>3</sup>. In this study, we are assuming a specific gravity of unity in the absence of additional data that would support a more accurate estimate.

The MOUDI and SMPS mass concentration data sets are shown in Table 4 and plotted in Figure 5. These mass concentration data have been corrected for the dilution factors shown in Table 2, so that the mass concentrations are estimated tailpipe

values. Figure 5 indicates that the SMPS and MOUDI particulate mass concentrations correlate with an r-squared (coefficient of determination) value of 0.90.

Carbon particulate data were obtained by summing the measurements obtained by exposing aluminum foil substrates in MOUDI impactor #2. Elemental carbon (EC) and organic carbon (OC) were determined according to the empirical thermal

Table 4  
Particulate mass and carbon concentrations

Run number	SMPS mass concentration, $\mu\text{g}/\text{m}^3$	MOUDI mass concentration, $\mu\text{g}/\text{m}^3$	MOUDI EC concentration, $\mu\text{g}/\text{m}^3$	MOUDI OC concentration, $\mu\text{g}/\text{m}^3$	MOUDI total carbon concentration, $\mu\text{g}/\text{m}^3$
5	1.53E+3	3.67E+3	5.45E+2	8.04E+2	1.35E+3
6	2.02E+3	3.12E+3	3.90E+2	9.64E+2	1.35E+3
7	6.72E+3	7.63E+3	1.80E+3	5.40E+3	7.20E+3
8	1.47E+3	2.39E+3	5.46E+2	9.94E+2	1.54E+3
9	3.88E+3	5.33E+3			
10	1.01E+4	1.23E+4	3.19E+3	1.33E+4	1.65E+4
12	1.37E+4	2.30E+4	7.58E+3	1.79E+4	2.55E+4
13	3.62E+4	3.19E+4	2.89E+3	2.09E+4	2.38E+4

MOUDI data were not obtained for Run 11. Carbon analyses were not performed for Run 9.

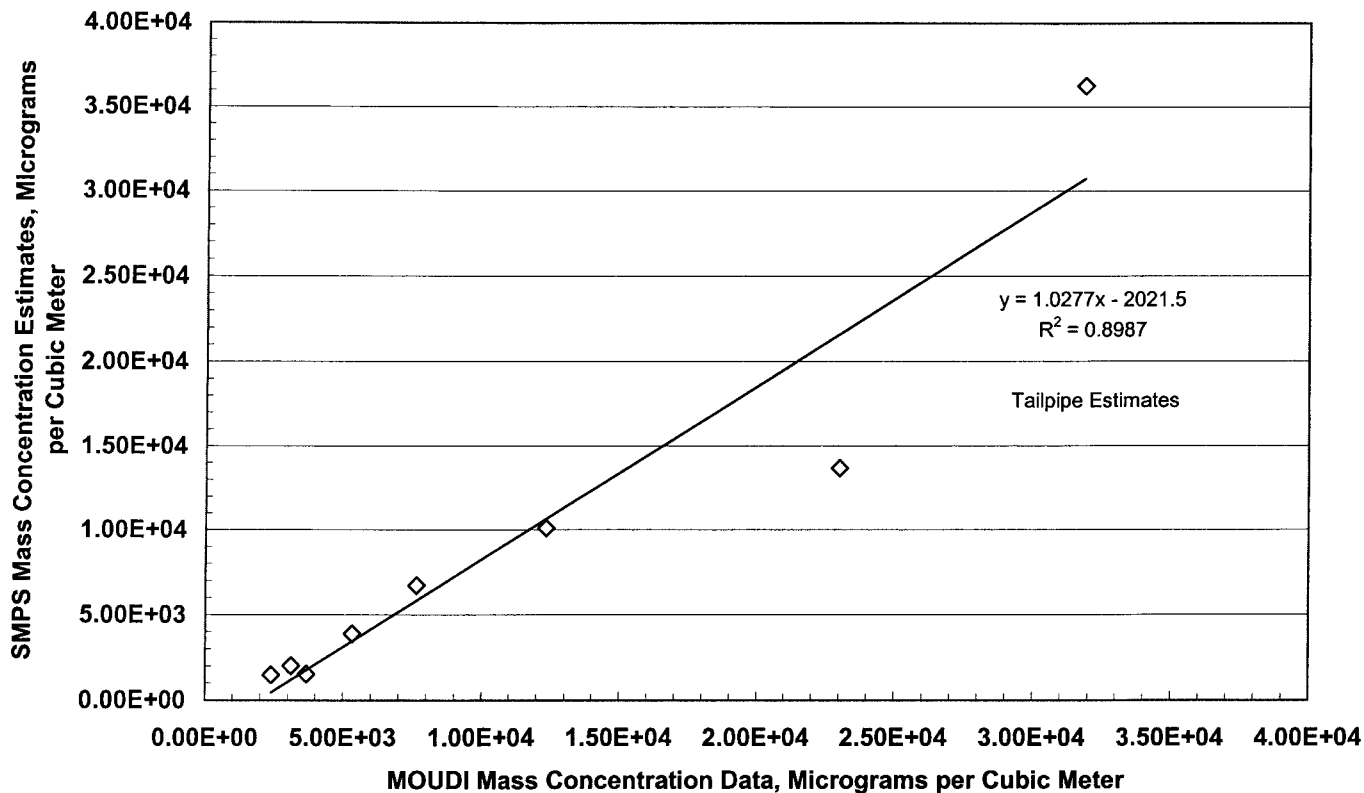


Figure 5. Comparison of MOUDI gravimetric mass concentrations and SMPS-derived estimates.

ramp method (Chow et al. 1993). MOUDI afterfilter data are not included in the carbon sums shown in Table 4 because the afterfilter is subject to artifact adsorption of vapor phase organic material. The OC concentrations obtained from the MOUDI runs were multiplied by a factor of 1.17 in order to estimate the reconstructed mass associated with the “organic” compounds (Pierson and Brachaczek 1983). MOUDI carbon data are not available for Runs 9 and 11. Figure 6 shows the regression of the MOUDI-derived carbon sums (EC + OC) against the MOUDI-derived  $PM_{2.5}$  mass concentrations for the available data. The slope of the regression in Figure 6 indicates that the summed carbon mass accounts for about 89% of the  $PM_{2.5}$  mass, with an r-squared value of 0.88. The arithmetic average of the ratios, OC + EC/gravimetric mass for all MOUDI runs is 0.80 with a standard deviation of 0.35. Including the masses of particulate elements from sodium to uranium, and nitrate, sulfate, and ammonium ions changes the slope of the regression line and the r-squared value in Figure 6 by less than the measurement uncertainties.

Uncertainty estimates for these data are presented in Appendix B. The relative precisions of the SMPS mass concentration measurements range from 12% to 17% without including any uncertainty component associated with the assumed particle density. The relative precisions of the MOUDI mass concentration measurements range from 3% to 23%, and the relative

precisions of the MOUDI carbon measurements range from 4% to 10%.

## DISCUSSION

### Size Distribution Data

The size distribution data from Run 5 (Figure 1) are quite similar in form to on-road observations in situations dominated by heavy-duty diesel trucks (e.g., Abu-Allaban et al. 2002). The CMD is 22 nm, close to the peak diameter and confirming that most of the number counts are in the nucleation mode. An accumulation mode seems to have developed as a discernable shoulder in the 50–100 nm region.

The size distribution data from the 1997 Coleman and the 1990 bobtail show a tendency for greater rpm values to generate larger particle sizes. For the 1997 Coleman, increasing the rpm setting from 800 to 1800 increased the CMD from 28 nm to 43 nm; the higher rpm run’s distribution indicates an emerging accumulation mode (Figure 2). For the 1990 bobtail (Figure 3), increasing the rpm setting from 750 to 1700 increased the CMD from 30 to 63 nm. The 1200 rpm data for this engine do not indicate that the CMD increased compared to the idle data, but an accumulation mode had emerged, and it dominated the distribution for the 1700 rpm case.

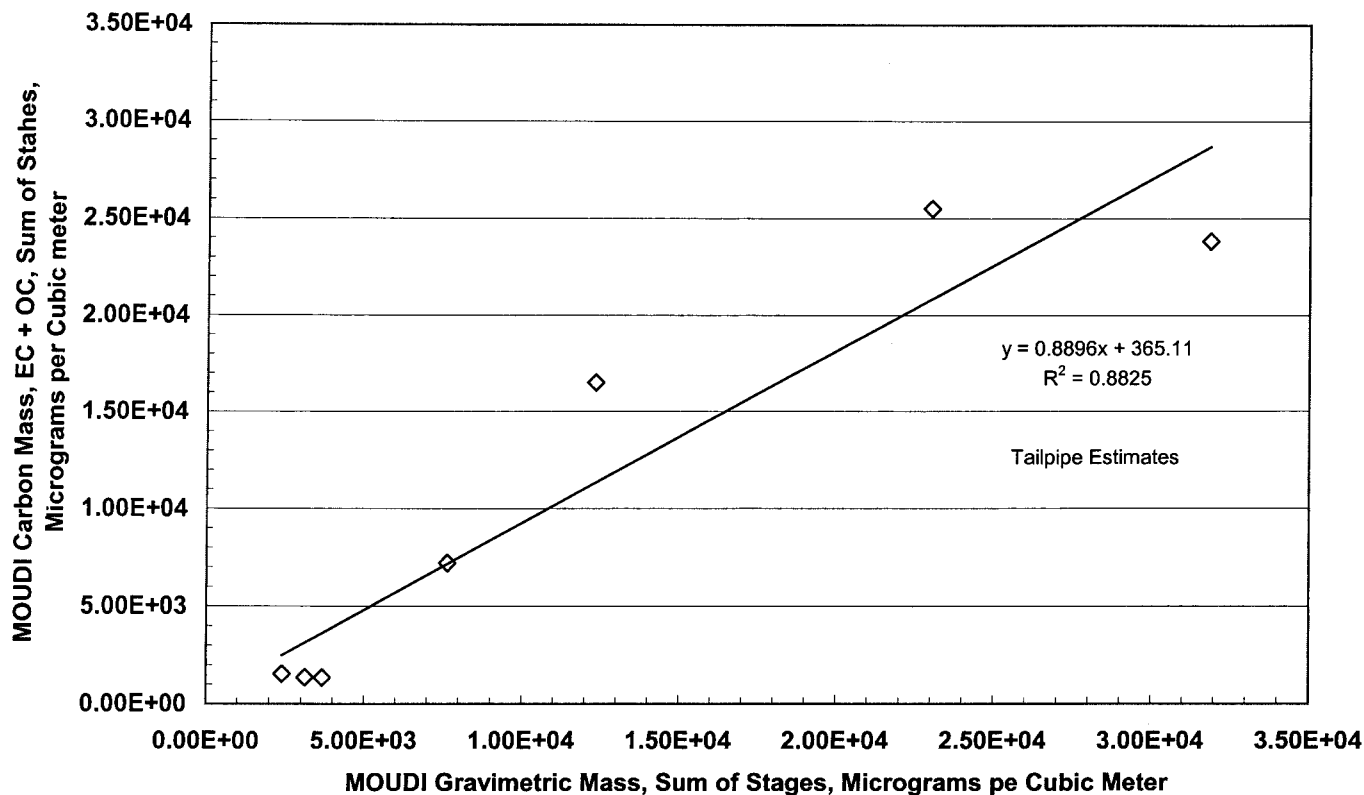


Figure 6. MOUDI particulate carbon mass compared to MOUDI gravimetric mass.

The relative growth of the accumulation mode compared to the nucleation mode as rpm increased was also observed by Abdul-Khalek et al. (1998), in tests of a 1995 direct injection, 4-liter Perkins engine running on fuel with a sulfur content of 300 to 412 ppm by weight. The tests utilized ISO 8-mode and 11-mode cycles; the engine was operated at a specified load and rpm for 10 min in each mode. This data obtained by these investigators was obtained with the engine at steady load and rpm settings during the measurement, which more closely resembles the HAFB procedure than would a variable drive cycle. The HAFB data are probably most comparable to the 10% load condition data from Abdul-Khalek et al. (1998). These investigators found 60% of the particles in the nucleation mode at 1600 rpm, but only 35% in the nucleation mode at 2600 rpm, illustrating the shift from the nucleation to the accumulation mode as the rpm increased.

Kittelson (1998) and Kittelson et al. (1999) have presented the "N/V" ratio as one means of parameterizing and comparing diesel exhaust particle size distribution measurements. For a given sample of the aerosol, N is the number of particles, and V is the volume of the particulate matter expressed in cubic micrometers ( $\mu\text{m}^3$ ). The diameter that is calculated from the V parameter is the diameter of average volume. (Note that increasing N/V ratios indicate a trend toward smaller particles in a sample.) Kittelson (1998, Figure 6) shows a comparison of the N/V ratios resulting from five previous diesel exhaust

studies and one previous spark-ignition exhaust study. For these cases, the diesel N/V ratios were a function of the fuel-air equivalence ratio; generally, the N/V values fell between about  $10^3$  and  $10^6 \mu\text{m}^{-3}$ , with most values less than  $10^5 \mu\text{m}^{-3}$ . For diesels, Kittelson (1998) finds the highest N/V ratios at the lowest fuel-air ratios, and hypothesizes that this results from the formation of nanoparticles by homogeneous nucleation. The values of the N/V ratios fall by roughly one order of magnitude as the fuel-air equivalence ratio increases from 0.2 to 1.0.

Although the fuel-air equivalence ratio was not measured for the HAFB tests, we can compare the N/V ratios from those tests to Kittelson's (1998) survey as one indication of the comparability of the HAFB results. Table 5 presents the N/V ratios and the diameter of average volume for all runs.

Table 5 confirms and quantifies the observation that larger particle sizes and expanding accumulation modes resulted for both the 1997 Coleman and the 1990 bobtail as the rpm settings were increased. For the 1997 Coleman, the N/V decreased and the diameter of average volume increased as the rpm setting was increased from 800 to 1800. For the 1990 bobtail, the rpm settings were 750, 1200, and 1700; as these settings increased, the N/V ratio decreased and the diameter of average volume increased monotonically. The JP-8 jammer results include the lowest N/V ratio and the largest diameter of average volume. For these tests the N/V ratios are within but near the low end of the range, and the diameters of average volume are within but

**Table 5**  
N/V ratios and diameters of average volume for HAFB tests

Run number	AGE vehicle	RPM	N/V ratio (particles per cubic micrometer)	Diameter of average volume (nm)
5	'96 Dodge Bobtail	800	$5.60 \times 10^3$	70
6	'97 Coleman	800	$8.55 \times 10^3$	61
7	'97 Coleman	1800	$3.64 \times 10^3$	81
8	'97 Coleman	800	$1.12 \times 10^4$	55
9	'90 Bobtail	750	$4.72 \times 10^3$	74
10	'90 Bobtail	1200	$1.58 \times 10^3$	106
11	'90 Bobtail	750	$3.04 \times 10^3$	86
12	'90 Bobtail	1700	$1.27 \times 10^3$	115
13	Jammer	2500	$9.62 \times 10^2$	126

Results are calculated for samples after dilution.

near the high end of the range presented in Kittelson (1998), for civilian diesel vehicle tests.

#### **Particulate Mass and Carbon Data**

As indicated by the data shown in Table 4 and Figure 5, the SMPS mass concentration estimates seem to explain the variations in mass that were found during Runs 5 through 13. The greatest mass concentrations measured for a given vehicle correspond to the highest rpm settings for the tests on that vehicle. The accumulation modes of the mass-size distributions from these test runs accounted for 79% to 99% of the total particle mass as estimated from the SMPS data. The variations in the accumulation modes seem to explain the observed differences in the integrated PM<sub>2.5</sub> mass concentrations from run to run.

With the exception of Run 13, the SMPS estimates of mass are lower than those from the MOUDI, as would be expected from the omission of particles larger than 352 nm. For Run 12, the PM<sub>2.5</sub> mass concentration derived from the MOUDI data is much greater than the SMPS estimate. In this case, the MOUDI data show an unusually high OC concentration on the two upper stages with cutpoints of 1.8 and 3.2  $\mu\text{m}$  (operated downstream from the 2.5  $\mu\text{m}$  cyclone), while the SMPS scan does not extend to diameters larger than 352 nm. Run 13 (JP-8 jammer) generated the greatest mass concentrations of the experiment.

The data in Table 4 lead to the conclusion that EC and OC constituted  $20 \pm 8\%$  and  $60 \pm 30\%$  (average and standard deviation), respectively, of the PM<sub>2.5</sub> mass generated by all of the engines in this study. The JP-8 jammer data (Run 13) are outliers in this calculation, with 9% EC and 66% OC. We hypothesize that the jammer exhaust may have included some particle-phase unburned fuel.

Kirchstetter et al. (1999) present on-road particulate carbon measurements that seem to approximate a fleet average. The findings of these investigators may be compared to the HAFB findings, although the latter are not intended to represent a fleet average. Kirchstetter et al. (1999) measured PM<sub>2.5</sub> mass, EC,

and, OC generated by traffic driving on a 4.2% uphill grade in the Caldecott Tunnel, near Oakland, California. EC and OC respectively comprised  $51 \pm 11\%$  and  $20 \pm 2\%$  of the PM<sub>2.5</sub> mass generated by heavy-duty diesel traffic. Therefore, the data that we have presented from the HAFB tests indicate that EC was a significantly smaller fraction of the PM<sub>2.5</sub> mass, while OC was a significantly greater fraction, than was found in the Caldecott Tunnel experiment (Kirchstetter et al. 1999). We hypothesize that this difference is attributable to the different external loads applied to the vehicles in the two studies. A qualitatively similar result has also been presented by Shi et al. (2000), who found that increasing the load on a diesel engine from 25% to 100% led to a factor of about 1.5 increase in EC and a factor of about 2.0 decrease in OC.

#### **Potential Measurement Artifacts**

We consider two types of measurement artifacts that might affect the particle size distribution observations: the removal of nucleation mode particles due to coagulation in the dilution sampler aging chamber, and the production of spurious particles in the sampling equipment.

The N/V ratio analysis discussed earlier in this paper led to particle diameters of average volume that were on the large end of the range reported by Kittelson (1998). This observation would be consistent with loss of nucleation mode particles through coagulation with accumulation mode occupants during their 80 s residence in the aging chamber of the dilution sampler. This process wouldn't affect summed particle mass concentrations, but would distort the size distributions.

To obtain an approximate estimate of the magnitude of the coagulation mechanism, we considered nucleation mode particles 20 nm in diameter coagulating with accumulation mode particles 100 nm in diameter. Average values for diesel exhaust particle number concentrations are  $5.8 \times 10^5 \text{ cm}^{-3}$  and  $3.3 \times 10^5 \text{ cm}^{-3}$  for the diluted nucleation and accumulation modes, respectively. The simple discrete coagulation equation and the coagulation

coefficient appropriate for 10 nm and 100 nm particles coagulating with each other (Seinfeld and Pandis 1998) can be applied in order to generate an approximate estimate. Assuming that every coagulation event removes a nucleation mode particle and transfers it to the accumulation mode, this approach indicates that somewhat less than 30% of the nucleation mode particles were affected by coagulation. Therefore, the nucleation mode concentrations that we observed in this study were underestimated by a factor on the order of 30% due to coagulation in the aging chamber. This finding would have no effect on the summed particle mass, and since the nucleation mode is only attenuated, not removed, the conclusions pertaining to the growth of the accumulation mode with increasing rpm are unaffected. Coagulation does, however, seem consistent with the N/V ratio discrepancies described earlier.

Recent studies have also identified conditions under which spurious particles may be produced in dynamometer dilutor sampling systems. Kittelson et al. (1999) report investigations into the effects of different dilution scenarios on the nucleation of particles after the exhaust has left the tailpipe. These investigators found that dilution ratios in the 10 to 50 range, at normal ambient temperatures and when achieved rapidly, are sufficient to initiate homogeneous nucleation of sulfuric acid. These researchers suggest that the most likely path for condensation of the soluble organic fraction is via heterogeneous nucleation onto the sulfuric acid particles. Dilution ratios that reach the 10 to 50 range but do not increase any further are appropriate for the formation of sulfuric acid particles by homogeneous nucleation. If the dilution continues rapidly past this range, the sulfuric acid supersaturation will not be maintained, and homogeneous nucleation will not be possible (Kittelson et al. 1999).

Maricq et al. (1999a), conducted dynamometer studies on passenger cars equipped with both gasoline and diesel engines, in order to identify potential artifacts in particle size distributions. Their studies utilized primary dilution ratios between 10 and 32. The findings of Maricq et al. (1999a) included the discovery that transfer hoses leading from the test vehicle to a dilution tunnel can act as "storage reservoirs" for semivolatile hydrocarbon compounds. If the transfer hose is insulated, it can later be heated by the exhaust gases enough that "stored" hydrocarbons are desorbed, forming spurious nuclei mode particles with high particle concentrations.

The dilution sampler at HAFB utilized dilution ratios of 1:18 to 1:20 (sample air to clean air). The dilution sampler inlet line was heated to 100°C and kept at that temperature by a controller; it was also replaced after Run 9. One consistent consequence of either spurious homogeneous nucleation or transfer line desorption seems to be the creation of nucleation mode particles. For homogeneously nucleated sulfuric acid, Kittelson et al. (1999) are not specific about particle sizes, stating only that the particles would fall in the nucleation mode. Maricq et al. (1999a) show examples of nucleation mode artifact "signals" in their Figures 4, 6, 7, 9, 10, and 11. The accumulation mode seems relatively unaffected.

Exhaust temperatures were measured at the inlet to the dilution sampler line during the HAFB tests; these data show that the exhaust temperature exceeded 100°C for Run 7 (152°C), and Run 12 (142°C). If the dilution sample inlet line was acting as a reservoir of adsorbed material for Run 12 as found in the Maricq et al. (1999a) study, one would expect to see high concentrations of particles in the nucleation modes of Runs 7 and 12, and possibly Runs 8 and 13. Instead, the SMPS data from Runs 7, 8, and 12 all seem to fit within the consistent pattern involving reduction of the nucleation mode and growth of the accumulation mode as the rpm setting was increased. Furthermore, the distribution for Run 13 does not exhibit high nucleation mode particle concentrations. The artifact formation process may have been operative but suppressed for Runs 12 and 13 because the inlet line was replaced after Run 9 and therefore was relatively clean.

The presence of artifact particles is not obvious in the remaining HAFB test runs. The 1997 Coleman and 1990 Bobtail test sequences (Runs 6–8 and 9–12) indicate that the nucleation mode particle concentrations actually decrease with increasing rpm, which seems contrary to the behavior one would expect from the artifact formation processes. These observations do not contradict the artifact scenarios and well-justified recommendations presented by Kittelson (1999) and Maricq et al. (1999). Rather, they suggest that the transfer line and dilution conditions during the HAFB tests avoided spurious particle production phenomena to a reasonable degree.

## SUMMARY AND CONCLUSIONS

The AGE vehicle tests conducted at Hill Air Force Base in September 1999 included three diesel-fueled vehicles, and one vehicle operating on JP-8 aviation fuel. The results of nine test runs are reported. The rpm settings were kept constant during the runs and no external loads were imposed.

The measured particle size distributions generally varied little during the 45 min test runs. The averaged number-size distribution data exhibited modes peaking between 21 and 84 nm. Not all distributions include clearly discernable accumulation modes. The low-rpm number-size distributions were often qualitatively similar in form to on-road distributions obtained in situations dominated by heavy-duty diesel trucks. The Count Median Diameters (CMD) of the distributions obtained in these tests increased as the engine rpm increased, indicating a shift from the nucleation mode to the accumulation mode as rpm was increased.

The number-size distributions reported here were utilized to calculate "N/V" ratios (Kittelson 1998), and to examine the shifting proportions of nucleation and accumulation mode particles as the rpm was varied. The N/V ratios and diameters of average volume for the HAFB diesel data fall in the same ranges found by Kittelson (1998) in a survey of four earlier studies on civilian engines operating at fuel-air equivalence ratios less than 0.6. For two of the diesel vehicles for which low and high rpm tests were conducted, the accumulation mode includes more of the particle population at the higher rpm setting compared to

the lower setting. This finding is consistent with the low-load, constant-rpm data presented by Abdul-Khalek et al. (1998) for a civilian diesel engine.

The SMPS number-size distribution data, when converted to mass concentration estimates by assuming a specific gravity of one, reproduce the trends shown in most of the test sequences. For any one vehicle tested, increasing the rpm resulted in increased  $PM_{2.5}$  mass concentrations. When measured  $PM_{2.5}$  mass concentrations exhibit larger values, those maxima are related to the growth of accumulation modes in the size distributions. Accumulation mode particles accounted for 79% to 99% of the summed particle mass based on the SMPS data.

A MOUDI cascade impactor was also used to measure  $PM_{2.5}$  particle mass concentrations, as well as carbon constituents determined by the Thermal-Optical Reflectance method. The measured  $PM_{2.5}$  mass concentrations varied greatly from one vehicle to the next. The mass concentrations determined by the two methods correlate well, with a slope of 1.03 and an r-squared value of 0.90. When MOUDI determinations of particulate carbon constituents, EC and OC, are plotted against MOUDI particulate mass, the regression slope is 0.89 and the r-squared value is 0.88.

The HAFB data were compared to other recently published data in order to assess their comparability. Since the HAFB data were obtained with constant rpm settings but no imposed loads, previously published drive cycle or on-road data are not directly comparable. The HAFB data indicate that EC contributed less and OC contributed more to the  $PM_{2.5}$  mass than in data sets obtained in studies involving engine operation under load.

The sampling procedure utilized for the HAFB SMPS measurements included 80 s of aging of the diluted aerosol prior to sampling. Coagulation of nucleation mode particles with the accumulation mode resulted in attenuation of the nucleation mode concentrations by factors on the order of 30%. This process does not affect the analyses of summed particle masses and the contribution of carbon species to them.

The sampling procedure also may have involved artifact particle formation, according to recent studies obtained after the experiment. Kittelson et al. (1999) and Maricq et al. (1999a) discuss artifact particle formation due to spurious homogeneous nucleation of sulfuric acid and to the storage and release of semivolatile compounds by transfer lines that conduct hot exhaust to dilution systems. The consistent feature of these artifacts is the generation of spurious nucleation mode particles. The HAFB SMPS data set generally does not seem to display evidence of spurious nucleation mode particles. If such particles are present, they are quite difficult to distinguish from "real" particle modes that might well be expected based on comparison data, such as on-road studies of heavy-duty diesel exhaust.

## REFERENCES

Abdul-Khalek, I. S., Kittelson, D. B., Graskow, B. R., Wei, Q., and Brear, F. (1998). Diesel Exhaust Particle Size: Measurement Issues and Trends. Paper number 980525, Society of Automotive Engineers.

- Abu-Allaban, M., Coulomb, W., Gertler, A. W., Gillies, J., Pierson, W. R., Rogers, C. F., Sagebiel, J. C., and Tarnay, L. (2002). Exhaust Particle Size Distribution Measurements at the Tuscarora Mountain Tunnel, *Aerosol Sci. Technol.* 36:771–789.
- Baumgard, K. J., and Johnson, J. H. (1996). The Effect of Fuel and Engine Design on Diesel Exhaust Particle Size Distributions. SAE Technical Paper 960131, SAE International, Warrendale, PA.
- Bevington, P. R., and Robinson, D. K. (1992). *Data Reduction and Error Analysis for the Physical Sciences*, Second Edition. McGraw-Hill, New York.
- Chow, J. C., Watson, J. G., Pritchett, L. C., Pierson, W. R., Frazier, C. A., and Purcell, R. G. (1993). The DRI Thermal/Optical Reflectance Carbon Analysis System: Description, Evaluation, and Application in U.S. Air Quality Studies, *Atmos. Environ.* 27A:1185–1202.
- Hildemann, L. M., Cass, G. R., and Markowski, G. R. (1989). A Dilution Stack Sampler for Collection of Organic Aerosol Emissions: Design, Characterization, and Field Tests, *Aerosol Sci. Technol.* 10:193–204.
- Hinds, W. C. (1999). *Aerosol Technology*, 2nd Edition. Wiley-Interscience, New York.
- Kinney, P. D., Pui, D. Y. H., Mulholland, G. W., and Bryner, N. P. (1991). Use of Electrostatic Classification Method to Size 0.1  $\mu\text{m}$  SRM Particles—A Feasibility Study, *J. Res. Natl. Stand. Technol.* 96(2):147–176.
- Kirschstetter, T. W., Harley, R. A., Kreisberg, N. M., Stolzenburg, M. R., and Hering, S. V. (1999). On-Road Measurement of Fine Particle and Nitrogen Oxide Emissions from Light- and Heavy-Duty Motor Vehicles, *Atmos. Environ.* 33:2955–2968.
- Kittelson, D. B. (1998). Engines and Nanoparticles: A Review, *J. Aerosol Sci.* 29:575–588.
- Kittelson, D. B., Arnold, M., and Watts, W. F. (1999). Review of Diesel Particulate Matter Sampling Methods, Final Report, University of Minnesota, Department of Mechanical Engineering, Center for Diesel Research, Minneapolis, MN.
- Kittelson, D. B. (2002). Personal Communication.
- Kleeman, M. J., Schauer, J. J., and Cass, G. R. (2000). Size and Composition Distribution of Fine Particulate Matter Emitted from Motor Vehicles, *Environ. Sci. Technol.* 34:1132–1142.
- Lighty, J. S., Veranth, J. M., and Sarofim, A. F. (2000). Combustion Aerosols: Factors Governing Their Size and Composition and Implications to Human Health, Critical Review, *J. Air & Waste Manage. Assoc.* 50:1565–1618.
- Maricq, M. M., Chase, R. E., Podsiadlik, D. H., and Vogt, R. (1999a). Vehicle Exhaust Particle Size Distributions: A Comparison of Tailpipe and Dilution Tunnel Measurements. SAE paper 1999-01-1461, Society of Automotive Engineers.
- Maricq, M. M., Podsiadlik, D. H., and Chase, R. E. (1999b). Examination of the Size-Resolved and Transient Nature of Motor Vehicle Particle Emissions, *Environ. Sci. Technol.* 33:1618–1626.
- Pierson, W. R., and Brachaczek, W. W. (1983). Particulate Matter Associated with Vehicles on the Road. II, *Aerosol Sci. Technol.* 2:1–40.
- Seinfeld, J. H., and Pandis, S. N. (1998). *Atmospheric Chemistry and Physics*. John Wiley and Sons, New York.
- Shi, J. P., Mark, D., and Harrison, R. M. (2000). Characterization of Particles from a Current Technology Heavy-Duty Diesel Engine, *Environ. Sci. Technol.* 34:748–755.
- Wang, S. C., and Flagan, R. C. (1990). Scanning Electrical Mobility Spectrometer, *Aerosol Sci. Technol.* 13:230–240.

## APPENDIX A

### Details of Dilution Sampler

The web site [www.das.dri.edu/OAL/DilutionSampler.html](http://www.das.dri.edu/OAL/DilutionSampler.html) includes a diagram of the dilution sampler. The inlet to the

dilution sampler was a 1.08 cm inside diameter, 320 cm long line actively controlled to 100°C wall temperature. At the downstream end of this line, flow was measured by a venturi with pressure taps (Lambda Square, Inc., Bay Shore, NY, similar to the example shown in Figure 2.9 in Hinds 1999). For the measurements we report here, the sample line flow ranged from 35 to 38 l/m. Accordingly, the transit time for the sample, from the tailpipe to the venturi, was about 0.47 to 0.50 s in turbulent flow, with Reynolds Numbers ranging from about 2900 to 3200.

Upon exiting the venturi, the sample flow was immediately delivered to the side wall of a 15 cm diameter cylindrical duct carrying ambient air used for dilution. The dilution air was filtered and passed through an activated carbon bed prior to mixing with the exhaust sample flow. The ambient air temperatures varied only over an 11°C range, from 20° to 31°C. For this experiment, the dilution air flows ranged from 680 to 710 l/m. The flow was therefore turbulent, with Reynolds Numbers ranging from about 5500 to 5700. The 15 cm duct carried the mixed sample and dilution flows over a distance of about 274 cm before part of the mixed flow was diverted into the top of an aging chamber. The transit time of the mixed flow, from the venturi outlet to the aging chamber connection, therefore ranged from 3.9 to 4.1 s.

The aging chamber was a stainless steel cylinder, 46 cm in diameter and 300 liters in volume, at ambient temperature. The flow through the aging chamber was the sum of two 113 l/m cyclone (Bendix-Unico 240 units, 2.5 μm cutpoint, located at the bottom of the aging chamber) flows, plus about 4 l/m from exit ports that did not utilize cyclones. Therefore, the average residence time in the aging chamber was about 80 s. The temperatures of the diluted exhaust samples ranged from 21° to 33°C, and the diluted sample relative humidities ranged from 16% to 25%.

The dilution ratios for each run are shown in the last column of Table 2. Each dilution ratio was calculated by taking the ratio of the total flow through the 15 cm mixing tube to the incoming sample flow as measured by the venturi. The venturi flow rate

has been corrected for the 100°C temperature of the sample flow. Since the estimated uncertainty in the venturi and sampling flows was ±5%, and the uncertainty in the main flow in the u-tube was ±10%, the propagated uncertainty of the dilution ratio was estimated to be about ±9%.

## APPENDIX B

### Measurement Uncertainties

*SMPS Precision.* Each of our test runs involved either six or seven SMPS scans, each of which utilized a 60 s up scan time and a 30 s down scan time. Time was also allowed in between scans, so that the SMPS was flushed from its previous run. Table B-1 summarizes three measures of the precisions of these measurements.

The third column in Table B-1 is the average over the given number of SMPS scans of the summed particle number concentrations. The fourth column is the standard deviation of the individual summed number concentrations, expressed as a percentage of the average (relative standard deviation). We utilize standard deviations and relative standard deviations as measures of measurement precision. The fifth column is the average over the given number of SMPS scans of the Count Median Diameter (CMD), as calculated by the SMPS software (version 2.4, TSI, Inc, St. Paul, MN). The sixth column of the table shows the relative standard deviations of the CMD estimates. The seventh column of Table B-1 lists the averages of the geometric standard deviations ( $\sigma_g$ ) of the particle distributions, again as calculated by the SMPS software. The last column of the table lists the relative standard deviations of the  $\sigma_g$  estimates. The CMD and  $\sigma_g$  estimates assume that the particle size distributions consist of a single lognormal mode constrained by requiring that the summed particle concentration must equal the measured value. This assumption is not always strictly justified for the cases discussed here, because the distributions sometimes include a second mode. However, the estimated CMD is often close to

**Table B-1**  
Precision estimates for SMPS data

Run number	Number of SMPS scans	Average summed particle number concentration, (cm <sup>-3</sup> )	Relative standard deviation of summed concentration (%)	Average count median diameter (CMD), nm	Relative standard deviation, CMD (%)	Average geometric standard deviation of distribution ( $\sigma_g$ )	Relative standard deviation of $\sigma_g$ (%)
5	7	4.77E+5	13.7	23	5.1	1.94	3.6
6	7	8.95E+5	13.7	29	5.6	1.76	5.0
7	7	1.31E+6	14.3	44	16.3	1.76	2.2
8	6	8.39E+5	5.1	28	5.0	1.71	0.9
9	7	9.55E+5	21.0	27	2.4	1.86	0.8
10	7	8.55E+5	12.3	30	3.2	2.31	5.8
11	6	1.11E+6	4.6	31	0.9	1.89	3.3
12	7	9.17E+5	8.4	65	5.0	2.01	1.4
13	7	1.94E+6	7.9	86	5.2	1.67	0.8

the diameter of the main peak in the distribution, indicating that the lognormal fit is a conditionally useable approximation to the measured distribution.

Table B-1 shows that, as quantified by the relative standard deviations, the average summed number concentrations vary by 5% to 21% over the course of any one run, the CMD varies by 1% to 16%, and the  $\sigma_g$  varies from 1% to 6%. This estimate of the precision in the CMD measurement overlaps the SMPS size resolution estimate given by Maricq et al. (1999),  $\pm 0.5$  nm at 15 nm, to  $\pm 30$  nm at 500 nm. The relative precisions of the  $\sigma_g$  measurements indicate that the widths of these distributions varied less than their peak diameters and their number concentrations. These variations take account of both the measurement precision of the SMPS instrument, and any variations in the vehicle exhaust that might have occurred over the 45 min runs.

The summed particle mass in a distribution could be estimated by using a Hatch-Choate lognormal distribution relation to calculate the particle diameter of average mass (Hinds 1999). If the distributions obtained in this study consisted of a single lognormal mode, this approach would allow use of the precisions in Table B-1, and straightforward error propagation in order to estimate the summed particle mass precision. However, even though the accumulation modes are usually much smaller in particle concentrations than the corresponding nucleation modes, most of the particle mass is to be found there. It therefore seems somewhat inappropriate to use a Hatch-Choate relation with its assumption that a single lognormal mode fits the observed distribution.

We therefore calculated the summed particle mass uncertainty by propagating the uncertainty associated with each of the 51 channels of the SMPS averaged distributions, following the standard rules for error propagation (e.g., Bevington and Robinson 1992). It is instructive to consider a relative uncertainty of 100% in each channel's particle number count. This value is very conservative, i.e., probably overestimated, especially given that the square roots of the differential particle numbers in each channel, corresponding to a simple  $\sqrt{N}$  count uncertainty, were always less than 10%. However, when propagated over the 51 channels of the distributions, this estimate of the per-channel uncertainty leads to a summed number count uncertainty of  $\pm 16\%$  to  $\pm 20\%$ , which overlaps the upper range of relative standard deviations in summed number concentrations displayed in Table B-1. (Sample flow uncertainty also contributes to the number concentration uncertainty, but it is reasonable to assume that relative flow uncertainty is 5% or less, leading to second-order contributions in these cases.) The summed number count uncertainty estimate of  $\pm 16\%$  to  $\pm 20\%$  is also consistent with the observation (Kittelson 2002) that SMPS integrated number concentrations generally agree with well-calibrated condensation particle counters to within about 20%.

Table B-2 lists the summed SMPS particle mass concentration estimates and their propagated relative uncertainties de-

**Table B-2**  
SMPS mass concentration precision estimates

Run number	SMPS summed mass concentration, $\mu\text{g}/\text{m}^3$	Relative uncertainty, percent
5	1.53E+3	20.6
6	2.02E+3	18.5
7	6.72E+3	19.0
8	1.47E+3	17.2
9	3.88E+3	21.5
10	1.01E+4	24.3
11	6.59E+3	23.6
12	1.37E+4	21.7
13	3.63E+4	21.6

rived by the approach that has just been described. (These uncertainty estimates do not take particle density uncertainties into account.) For comparison, the Hatch-Choate relation mentioned earlier, and the precisions listed in Table B-1, were also used to estimate SMPS particle mass concentration uncertainties. The Hatch-Choate values exceeded those in Table B-2 by 0.1 to 4.0 relative uncertainty percent, indicating that the two methods agree within a factor of about 1.3.

Maricq et al. (1999a) estimated that the  $\pm 2\sigma$  uncertainty in exhaust particle mass emission rates derived from SMPS number-size distributions was  $\pm 50\%$ . These investigators stated that test-to-test variability and particle density uncertainty contribute approximately equally to their uncertainty estimate. The  $\pm 2\sigma$  estimates implied by our propagated precisions lie in the  $\pm 34\%$  to  $\pm 48\%$  range without including any measure of density uncertainty. Therefore, our mass concentration uncertainty estimates in Table B-2 are somewhat greater than the test-to-test variability components estimated by Maricq et al. (1999a).

*SMPS Accuracy.* At this time, there do not seem to be commonly accepted methods for checking SMPS number-size distribution accuracies. Kinney et al. (1991) found that the absolute accuracy with which particle diameters can be determined by electrostatic classifiers is about 3%. However, the particle sizing accuracy in an SMPS system is a function of the particle transit time from the classifier to the particle counter ("delay time"), as well as the classifier itself. If nonstandard tubing connections are used, or if for any other reason the aerosol transit time differs from that assumed by the SMPS software, then the particle sizing accuracy will be affected.

The absolute accuracy in particle number count determinations by the SMPS is just that of the Condensation Particle Counter (CPC, Model 3022A, TSI, Inc., St. Paul, MN) as long as the SMPS is operating properly. The manufacturer states that the absolute accuracy in CPC particle counts can be estimated by the square root of the count obtained in a given interval. The count accuracy has to be combined with the CPC flow rate

**Table B-3**  
MOUDI mass and total carbon measurement precisions

Run number	MOUDI mass concentration, $\mu\text{g}/\text{m}^3$	MOUDI mass concentration, relative precision, percent	MOUDI total carbon concentration, $\mu\text{g}/\text{m}^3$	MOUDI total carbon concentration, relative precision, percent
5	3.67E+3	13.0	1.35E+3	9.2
6	3.12E+3	16.4	1.35E+3	9.6
7	7.63E+3	6.9	7.20E+3	4.4
8	2.39E+3	23.1	1.54E+3	8.7
9	5.33E+3	10.2		
10	1.23E+4	5.2	1.65E+4	4.9
12	2.30E+4	3.6	2.55E+4	4.1
13	3.19E+4	3.5	2.38E+4	4.1

accuracy in order to derive the propagated accuracy of the particle concentration measurement.

*MOUDI Precision.* Table B-3 summarizes the measurement precisions calculated for the MOUDI mass and total carbon concentration measurements.

The precision estimates shown in Table B-3 are the result of propagating laboratory mass and carbon analysis precisions and estimated 5% sample flow precision. These propagated precisions decrease as the net amount of particulate material increases, as would be expected.

*MOUDI Accuracy.* The accuracies with which particulate mass and carbon concentrations are determined using cascade impactor samples depend on the application of traceable standards in the corresponding laboratory procedures. The microbalances used in this study were systematically calibrated with traceable gravimetric standards having an accuracy of  $\pm 5$  micrograms. Chow et al. (1993) state that the accuracy of the total carbon determination is  $\pm 5\%$ , and that the precision (not the accuracy) with which the "split" between OC and EC is determined is also  $\pm 5\%$ .